electronics

Article

Research on the Signal Noise Reduction Method of Fish Electrophysiological Behavior Based on CEEMDAN with Improved Wavelet Thresholding

Jingfei Meng [1,2,3], Weiming Cai [2,3,*], Siyi Ou [2], Jian Zhao [4], Shengli Fan [2,3] and Bicong Zheng [2,3]

1 School of Information Science and Engineering, Zhejiang Sci-Tech University, Hangzhou 310018, China
2 Signal Intelligence Detection and Life Behavior Perception Institute, NingboTech University, Ningbo 315100, China
3 Zhejiang Engineering Research Center for Intelligent Marine Ranch Equipment, Ningbo 315100, China
4 College of Biosystems Engineering and Food Science, Zhejiang University, Hangzhou 310058, China
* Correspondence: caiwm@nit.zju.edu.cn

Abstract: Electrophysiological signals are one of the key ways that fish convey information and govern movement. Changes in physiological electrical signals may indirectly reflect changes in fish sensory thresholds and locomotor behavior. The acquisition of physiological electrical signals in fish is more susceptible than in mammals to the effects of surface mucus and water noise, thereby reducing signal quality. In this study, a noise reduction method for electrophysiological behavioral signals in fish was proposed, namely the decomposition of the original EMG signal into multiple intrinsic mode components using CEEMDAN. To choose the signal-dominated IMF, noise-dominated IMF, and pure IMF, mutual correlation function characteristic analysis is done on each IMF and the original signal. The signal-dominated IMF is then filtered using the improved wavelet thresholding approach. Finally, the wavelet threshold filtered signal-dominated IMF with pure IMF was reconstructed into the processed fish EMG signal. It is demonstrated that the algorithm proposed in this paper improves the SNR by 3.1977 dB and reduces the RMSE by 0.0235 when compared to the traditional wavelet threshold denoising. The denoising method proposed in this paper can effectively improve the signal quality and provides an effective tool for the in-depth analysis of fish behavior from the perspective of physiological electrical signals.

Keywords: fish electromyographic signal; fish behavior; signal processing; CEEMDAN; wavelet threshold

check for updates

Citation: Meng, J.; Cai, W.; Ou, S.; Zhao, J.; Fan, S.; Zheng, B. Research on the Signal Noise Reduction Method of Fish Electrophysiological Behavior Based on CEEMDAN with Improved Wavelet Thresholding. *Electronics* **2023**, *12*, 4861. https://doi.org/10.3390/electronics12234861

Received: 22 October 2023
Revised: 28 November 2023
Accepted: 30 November 2023
Published: 1 December 2023

1. Introduction

Fish behavior is closely related to the muscles of the corresponding functional area, which perform movements by contraction and relaxation. The rapid tail wagging of fish is often used to catch prey and escape themselves, and is biologically important [1]. Neurobehavioral science attempts to reveal the neural mechanisms behind natural behavior, and the study of the correlation between neural activity and behavioral representations is challenging [2]. Fish use their muscles to propel them when they swim. To bend their bodies and swing their tails, the muscles on either side of the fish must alternately contract and relax. It was discovered by examining the EMG signals at anterior, middle, and posterior body locations in rainbow trout that the EMG signal appears at a more posterior position earlier in each tailbeat cycle [3]. EMG can detect, record and analyze the electrical signals of skeletal muscle contractions, it is also useful for measuring the degree of myocardial relaxation or contraction during the exposure of fish to the effects of exogenous anesthetic substances [4,5]. Cod exhibits transient epileptic-like impairment after being electrocuted, and the ECG signal will show high amplitude and high frequency waves during the tonic phase [6]. Differences in the behavior of different fish immersed in different concentrations of anesthetics were studied based on changes in delicate information such as EMG and ECG [7–9].

However, the collection of physiological electrical signals in fish is more susceptible to the effects of surface mucus, random noise in water and underwater dark current intensity than in mammals, thus reducing the signal quality. At present, the acquisition points of fish physiological electrical signals are not standardized, resulting in large random noise and a low signal noise ratio contained in the original fish physiological electrical signals. The poor signal quality makes it difficult to combine EMG, ECG and EEG signals for subsequent studies of fish behavior and physiology. The current fish muscle signal noise elimination process is usually a bandpass filter after the signal amplifier [10,11]. However, because relatively little is known about the inherent characteristics of the fish physiological electrical signal, choosing a filter with too wide or too narrow a bandwidth can lead to signal distortion and easily filter out critical parts of the signal. To address the issue of denoising such fish physiological electrical data, a signal processing approach more suited to noise removal from unknown signals should be adopted.

The empirical mode decomposition (EMD) is to decompose a segment of signal into some intrinsic mode function (IMF) and a residual function according to the time scale [12–14]. And the analysis of non-linear, non-smooth signals is appropriate for it [15,16]. EMD is widely used in the analysis of EMG and ECG signals in mammals such as humans for noise cancellation [17–19]. However, EMD is prone to the problem of modal mixing during the decomposition process [20]. To solve this problem, [21] proposed ensemble empirical mode decomposition (EEMD), adding random Gaussian white noise to the decomposition process to eliminate modal aliasing by the superposition of noise. Although EEMD can successfully reduce the modal mixing issue, it is challenging to completely remove the additional Gaussian white noise during the decomposition reconstruction phase, which lowers the data accuracy. To improve the accuracy, ref. [22] proposed complete ensemble empirical mode decomposition with adaptive noise (CEEMDAN). CEEMDAN is widely used in vibration signal denoising [23,24], ultrasound signal denoising [25], human ECG signal enhancement and other fields [26]. Using only CEEMDAN for noise reduction in the signal to be processed tends to discard the low-order components dominated by high-frequency noise, resulting in a partial loss of useful detail information. To solve this problem, wavelet thresholding is usually combined with EEMD, CEEMDAN, and applied to each signal denoising [27]. Simulation of heartbeat detection using CEEMDAN-WT denoising under different intensity EMG signal interference [28] in order to better restore the characteristics of the ECG signal, ref. [29] improved the wavelet thresholding and processed the actual ECG signal jointly with EEMD, and the experiments showed that the method could better preserve the characteristics of the signal.

This study proposes to combine the improved wavelet thresholding with CEEMDAN for application in the denoising of fish electrophysiological signals. Combined with the characteristics of fish EMG signals, this paper redesigned the wavelet threshold function and optimized the selection of IMF signals. Simulated denoising experiments are established to assess the denoising impact of the proposed algorithm based on SNR and RMSE. The actual noise cancellation of the acquired tail EMG signal is combined with the simple tail swinging behavior of the fish.

2. Materials and Methods

2.1. Experimental Animals

Crucian carp (450 ± 20 g, 25 ± 2 cm, total length) were purchased from a local commercial fishery and were temporarily housed in an 840 L rectangular glass aquarium equipped with an oxygenator, UV germicidal lamp and biofilter, under natural light. The tank was continuously aerated for oxygen supply, and the water quality parameters were maintained at (pH = 7.4 ± 0.2, temperature = 24.0 ± 1.0 °C, dissolved oxygen = 4 ± 1 mg/L and nitrite = 0.03 ± 0.01 mg/L). Prior to the research, these fish were hand fed twice each day (9:00 am and 17:00 pm) with feed components (crude protein ≥ 30%, crude fiber ≤ 14%, crude fat $\geq$ 3%), and no abnormal behavior for 3 days were considered as experimental fish. Feeding was stopped 24 h prior to the EMG signal acquisition experiment. All procedures were approved by the Experimental Animal Welfare Ethics Committee of Zhejiang University (project approval number: ZJU20190073).

2.2. EMG Recording

The electrodes were constructed with two 0.7 mm diameter insulated enameled copper wires, and the ends of the insulated enameled copper wires were stripped of paint by a (Huajin, HJ-220A, Dongguan, China) paint stripper before the experiment started. In experiments involving the acquisition of electrical signals from fish, it is difficult to standardize the location of electrodes implanted in muscle groups due to different experimental purposes, and the points chosen for this paper were determined after many experiments. One end of the electrode was bent into a hook shape with a diameter of 5 mm and attached to the dorsal lateral muscle fibers (15.0 mm below the mid-dorsal fin) and caudal lateral muscle fibers (5 mm above the mid-caudal lateral line). Its remote end is connected to a microvolt-level weak signal amplifier (Huigengsi, FA-300, Hangzhou, China) for data acquisition using a multifunctional data acquisition card (Smacq, USB-1252A, Beijing, China). The experimental sampling frequency was designed to detect the data continuously at 2 KHz and the Matlab 2020a software was used for filtering and analysis.

2.3. Signal Processing Processes and Methods

2.3.1. CEEMDAN Principle

EEMD is to perform EMD decomposition directly after adding white noise and calculate the average value directly for each order of IMF. After calculating the mean value of the first-order IMF, CEEMDAN adds Gaussian white noise to the residual IMF again, iteratively until the end. The detailed process is as follows [30,31]:

1. Adding Gaussian white noise with $\tau_0 \mathrm{w}^{\mathrm{i}}(t)$ normal distribution a to the original signal $x(t)$, then the signal of the i-th addition of Gaussian white noise $x^{\mathrm{i}}(t)$ is represented as:
$$x^{\mathrm{i}}(t) = x(t) + \tau_0 \mathrm{w}^{\mathrm{i}}(t) \tag{1}$$
τ_0 is the white noise coefficient, $\mathrm{w}^{\mathrm{i}}(t)$ is the i-th added white noise, and i is the number of trials.
2. Arithmetic averaging of the signal to be processed after one time repetition of decomposition using EMD yields the IMF_1 and the residual component $\mathrm{r}_1(t)$:
$$IMF_1(t) = \frac{1}{\mathrm{I}}\sum\nolimits_{\mathrm{i}=1}^{\mathrm{I}} \mathrm{E}_1\left[x^{\mathrm{i}}(\mathrm{t})\right] \tag{2}$$
$$r_1(t) = x(t) - IMF_1(t) \tag{3}$$
E is the operator of the intrinsic mode component obtained in the EMD of the signal to be processed.
3. Adding the standard normally distributed Gaussian white noise $\tau_1 \mathrm{w}^{\mathrm{i}}(t)$ to the residual component $r_1(t)$ and continuing the EMD, the $IMF_2(t)$ and the residual component $r_2(t)$ after removing $r_2(t)$ are expressed as:
$$IMF_2(t) = \frac{1}{\mathrm{I}}\sum\nolimits_{\mathrm{i}=1}^{\mathrm{I}} \mathrm{E}_1\left\{r_1(t) + \tau_1 \mathrm{E}_1\left[\omega^{\mathrm{i}}(\mathrm{t})\right]\right\} \tag{4}$$
$$r_2(t) = r_1(t) - IMF_2(t) \tag{5}$$
4. For l = 2, 3, . . ., L, the l-th residual component $r_l(t)$ is calculated as:
$$r_l(t) = r_{l-1}(t) - IMF_l(t) \tag{6}$$

5. The $IMF_{l+1}(t)$ of the extracted signal $r_l(t) + \tau_l E_l\left[\omega^i(t)\right]$ is expressed as:

$$IMF_{l+1}(t) = \frac{1}{I}\sum_{i=1}^{I} E_l\left\{r_l(t) + \tau_l E_l\left[\omega^i(t)\right]\right\} \tag{7}$$

6. Repeating steps 4 and 5 until the residual component signal is a monotonic function that can no longer be decomposed and eventually the L internal modal components may be acquired. It is possible to represent the original signal as follows:

$$x(t) = R(t) + \sum_{i=1}^{L} IMF_i(t) \tag{8}$$

2.3.2. Improvement of Wavelet Threshold Function

The signal may be split into low-frequency and high-frequency components, and it is commonly accepted that the high-frequency components of the signal contain the majority of the noise. The choice of an appropriate wavelet basis function and the amount of breakdown layers is the first step in wavelet threshold denoising. The electrical signal from the fish muscle that contains noise was wavelet decomposed to obtain a number of high-frequency wavelet coefficients and low-frequency wavelet coefficients. According to the characteristics of the wavelet transformed signal, a threshold setting rule is selected, and preserved wavelet coefficients with amplitudes larger than the predetermined threshold, and those with amplitude less than the set threshold are removed. Finally, the noise reduction signal is obtained by reconstructing the thresholding wavelet coefficients [32].

According to the principle of wavelet threshold denoising, it is known that after the wavelet decomposition, the fish electromyographic signal needs to be processed by the threshold function with noisy wavelet coefficients to remove the noise, and the threshold function's design is crucial for the signal denoising effect. Traditional wavelet coefficient processing algorithms have both hard and soft thresholding methods, with the following expressions:

1. Hard thresholding methods

$$\overline{\omega_{J,k}} = \begin{cases} \omega_{j,k} & , \left|\omega_{j,k}\right| \geq \lambda \\ 0 & , \left|\omega_{j,k}\right| < \lambda \end{cases} \tag{9}$$

2. Soft thresholding methods

$$\overline{\omega_{J,k}} = \begin{cases} \mathrm{sign}(\omega_{j,k})\left(\left|\omega_{j,k}\right| - \lambda\right) & , \left|\omega_{j,k}\right| \geq \lambda \\ 0 & , \left|\omega_{j,k}\right| < \lambda \end{cases} \tag{10}$$

In the field of practical research, both hard and soft thresholding have been extensively employed, nonetheless, both algorithms have flaws [33,34]. The signal's fundamental properties may be preserved to the fullest degree using the hard threshold function technique, but because the hard threshold function at $\pm\lambda$ is intermittent discontinuity, this intermittent discontinuity makes it easy for the signal to produce the pseudo-Gibbs phenomenon [35], and it is easy to generate oscillations when reconstructing the denoised fish EMG signal. The discontinuity of the hard thresholding approach is improved by the soft thresholding method, resulting in a smoother electrical signal from the denoised fish muscle. But there is a brand-new issue with fixed deviation among $\overline{\omega_{J,k}}$ and $\overline{\omega_{J,k}}$, which would diminish the SNR of the reconstructed fish EMG signal and lose some of the mutational information in the signal.

Considering the above problems, this paper improves on the former by introducing primary functions such as exponential functions and preset adjustable parameters α and β. The coefficients below the threshold in the wavelet decomposition are not immediately set to 0 and are instead provided modest compensation [36]. The following is the new wavelet threshold function expression that is presented in the study as an improved new wavelet threshold function:

$$\overline{\omega_{J,k}} = \begin{cases} \mathrm{sign}(\omega_{j,k})\left[\left|\omega_{j,k}\right| - \dfrac{\left|\omega_{j,k}\right| - \frac{\lambda}{\alpha}e^{\sqrt{\left|\omega_{j,k}\right|-\lambda}}}{e^{\beta\sqrt{\left|\omega_{j,k}\right|^2-\lambda^2}}}\right], & \left|\omega_{j,k}\right| \geq \lambda \\ \mathrm{sign}(\omega_{j,k})\dfrac{\left|\omega_{j,k}\right|}{\alpha}e^{\alpha\beta\left(\frac{\left|\omega_{j,k}\right|}{\lambda}-1\right)}, & \left|\omega_{j,k}\right| < \lambda \end{cases} \tag{11}$$

where λ is the threshold value, $\omega_{j,k}$ is the wavelet coefficient of the original signal, $\overline{\omega_{J,k}}$ is the new wavelet coefficient obtained after wavelet thresholding, and α and β are preset adjustable parameters. The schematic diagram of the traditional hard threshold, soft threshold, and enhanced threshold function curve in this research is shown in (Figure 1) below.

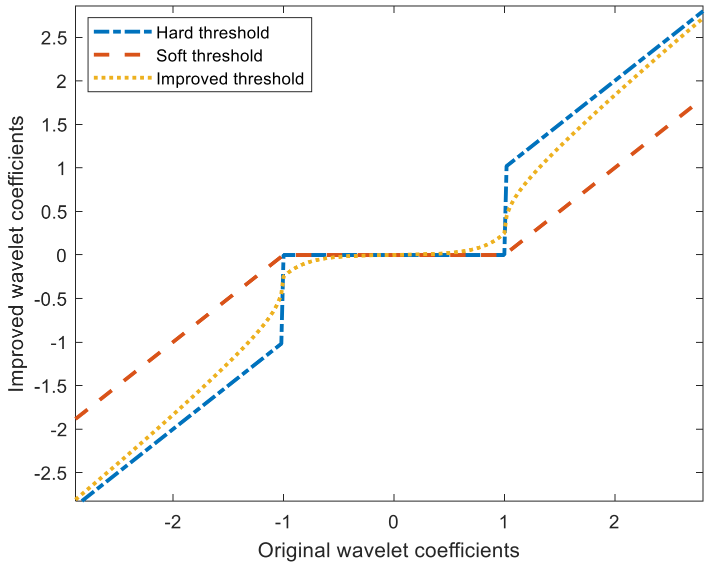

Figure 1. Comparison of three threshold functions (hard threshold, soft threshold, improved threshold).

The equation $f(\omega_{j,k}) = \overline{\omega_{J,k}}$, was created to check the improved threshold function's characteristics in the following five areas, and to demonstrate the function's viability using the mathematical justification [29]. The mathematical proof is derived as follows:

1. Parity

The function is in the range $(-\infty, +\infty)$, which is consistent with $f(\omega_{j,k}) = -f(-\omega_{j,k})$, so the function is an odd function.

2. Continuity

When $\left|\omega_{j,k}\right| = 0$, $f(\omega_{j,k}) = 0$, and when $\left|\omega_{j,k}\right| \to +\lambda$, $\lim\limits_{\omega_{j,k}\to\lambda^+} f(\omega_{j,k})$ $= \lim\limits_{\omega_{j,k}\to\lambda^+} \mathrm{sign}(\omega_{j,k}) * \left[\lambda^+ - \dfrac{\lambda^+ - \frac{\lambda}{\alpha}e^{\sqrt{\lambda^+-\lambda}}}{e^{\beta\sqrt{\lambda^{+2}-\lambda^2}}}\right] = \frac{\lambda}{\alpha}$. And when $\left|\omega_{j,k}\right| \to -\lambda$, $\lim\limits_{\omega_{j,k}\to\lambda^-} f(\omega_{j,k}) =$ $\lim\limits_{\omega_{j,k}\to\lambda^-} \mathrm{sign}(\omega_{j,k})\frac{\lambda^-}{\alpha}e^{\alpha\beta(\frac{\lambda^-}{\lambda}-1)} = \frac{\lambda}{\alpha}$.

The function satisfies the continuity at $\omega_{j,k} = \pm\lambda$, and the continuity of the function can improve the hard threshold function in signal reconstruction with oscillation, burr and other problems [37].

3. Progressivity

When $\left|\omega_{j,k}\right| \to +\infty$, $\lim\limits_{\omega_{j,k}\to\infty}\left[\frac{f(\omega_{j,k})}{\omega_{j,k}}\right] = \left[1 - \frac{\left|\omega_{j,k}\right| - \frac{\lambda}{\alpha}e^{\sqrt{|\omega_{j,k}|-\lambda}}}{\omega_{j,k} * e^{\beta\sqrt{|\omega_{j,k}|^2-\lambda^2}}}\right]$, and according to Lopita's law operation, $\lim\limits_{\omega_{j,k}\to\infty}\left[\frac{f(\omega_{j,k})}{\omega_{j,k}}\right] = 1$, it is demonstrated that when the wavelet coefficients steadily grow, this threshold function is asymptotic to the traditional hard threshold.

4. Constant difference

When $\left|\omega_{j,k}\right| \to +\infty$, $\lim\limits_{\omega_{j,k}\to+\infty}\left[f(\omega_{j,k}) - \omega_{j,k}\right] = \left|\omega_{j,k}\right| - \frac{\left|\omega_{j,k}\right| - \frac{\lambda}{\alpha}e^{\sqrt{|\omega_{j,k}|-\lambda}}}{e^{\beta\sqrt{|\omega_{j,k}|^2-\lambda^2}}} - \left|\omega_{j,k}\right| = 0$. Thus, it demonstrates that when wavelet coefficients are increased, the disparity between the reconstructed signal and the original signal gradually reduces.

5. Adjustable parameters

By modifying the preset parameters α and β, the threshold function may be flexibly altered. As shown in (Figure 2), when α = 2 and β = 2, the function graph converges to the hard threshold faster, and when α = 6 and β = 0.8, the function graph converges to the hard threshold function slower. The preset parameters can be adjusted appropriately according to the specific signal form to meet different needs.

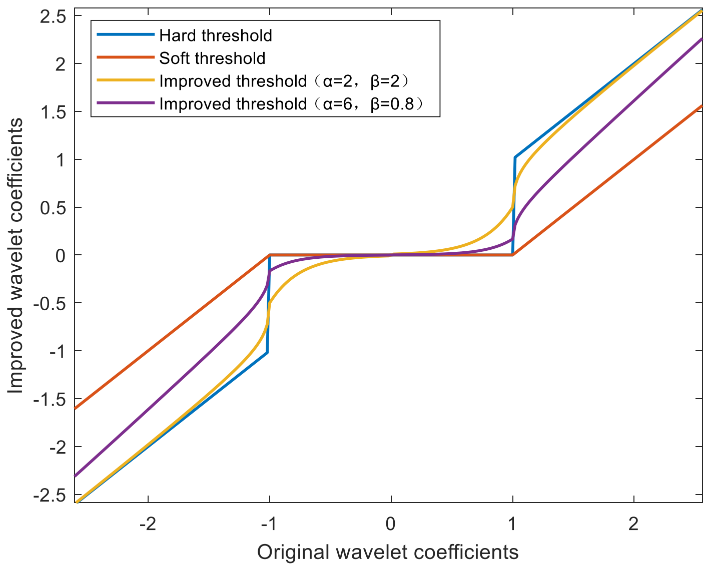

Figure 2. Improved threshold function schematic at different parameters (α = 2, β = 2; α = 6, β = 0.8).

2.4. CEEMDAN with Improved Wavelet Thresholding

The CEEMDAN-improved wavelet thresholding method first decomposes the fish tail EMG signal by CEEMDAN to obtain several IMFs with one residual component. How much relevance there is between each intrinsic mode component and the original signal is calculated, then the IMFs with the greatest and lowest correlations are filtered out. Although the IMF with the highest correlation will also contain some noise, it will also contain some weak signal details, so the IMF with the highest correlation is treated as the pure component. The minimum intercorrelation indicates a weak linear relationship between this IMF and the original signal, so this component is directly taken as the IMF dominated by noise. The difference of each correlation coefficient is calculated to obtain the difference curve, and the first extreme point past zero is selected according to the difference curve as the critical point between the noise-dominated IMF and the signal-dominated IMF [38]. The signal-dominated IMF is denoised via an improved wavelet thresholding approach to recover some of the useful information that is lost during the CEEMDAN decomposition process after the noise-dominated IMF and the pure noise component have been eliminated. Finally, the IMF is reconstructed with the pure component after improved wavelet thresholding to obtain the processed signal. The complete flow of the noise reduction algorithm is shown in (Figure 3).

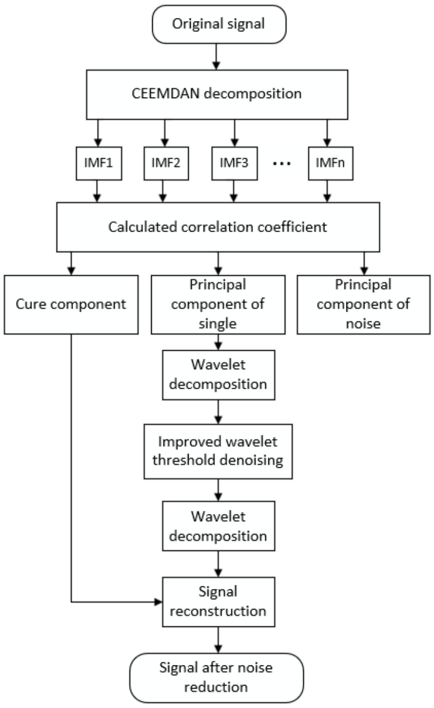

Figure 3. Signal processing flow.

3. Experiments and Results

3.1. Experimental Animals

Combining the features of the fish tail EMG signal, a part of the denoised fish EMG test signal was picked and 15 dB of random white noise was added to it, and the resulting noise-containing signal was filtered and tested using traditional wavelet threshold denoising, CEEMDAN with wavelet soft threshold denoising, CEEMDAN with wavelet hard threshold denoising, literature 1 [39] and literature 2 [40], and the study proposes using CEEMDAN with the improved wavelet threshold denoising technique.

The noise reduction effect is shown in (Figure 4), and it can be seen that different threshold functions have slightly different effects on signal denoising. (Figure 4A) shows the original test signal and (Figure 4B) shows the noise-containing signal with 15 dB of noise added to the original signal. The noise-containing signals were subjected to the following algorithms for noise removal simulation experiments, and the better algorithm is considered to be the one that can better recover the original signal characteristics. (Figure 4C) uses the traditional wavelet thresholding denoising algorithm, which can be seen to remove most of the noise, but there are still more burrs in some mutation details and incomplete noise filtering. Compared to the signal denoised directly by the wavelet threshold function, the signal decomposed by CEEMDAN and then denoised by the wavelet soft threshold function (Figure 4D) is generally smoother, but due to the introduction of the constant difference, the signal loses some detailed information at the mutation points. (Figure 4E) shows CEEMDAN decomposition followed by denoising using the wavelet hard thresholding function, however, this algorithm is not effective in detail burr suppression, but the details can be preserved. (Figure 4F,G) shows improved denoising algorithms where it can be seen that after processing combined with the fish electromyographic signal features, the noise-containing signals and the original signal are slightly different and there is still some room for improvement. (Figure 4H) shows the effect of the signal after CEEMDAN processing with the improved wavelet thresholding denoising method proposed in this paper, the algorithm retains the details in the original signal and removes the noise effectively, which is more similar to the original signal.

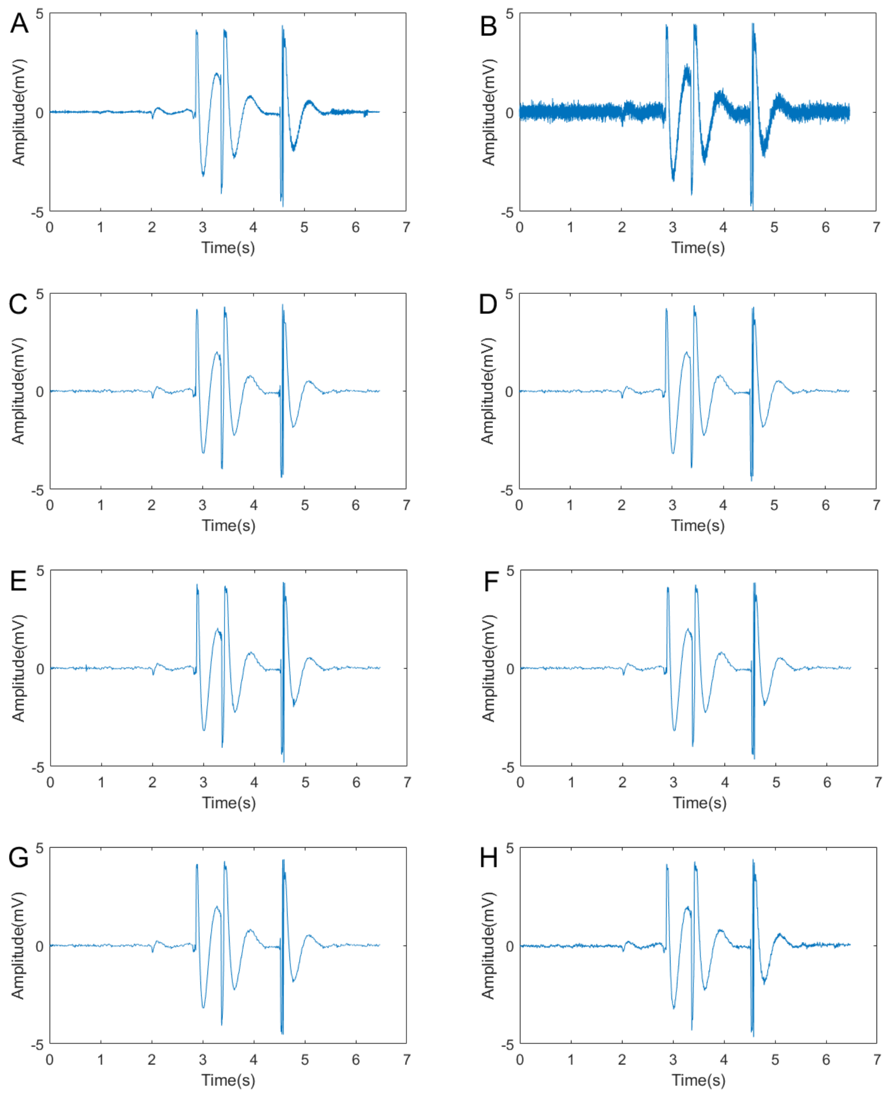

Figure 4. Comparison of noise reduction effects using different denoising algorithms. The original signal (**A**), 15 dB noise is added to the original signal to synthesize the noise-containing signal (**B**), after denoising using traditional wavelet thresholding (**C**), after denoising using CEEMDAN with wavelet soft threshold denoising (**D**), after denoising using CEEMDAN with wavelet hard threshold denoising (**E**), the denoising effect of other improved algorithms (**F**,**G**), the denoising effect of this algorithm (**H**).

In order to more intuitively portray the noise reduction impact of various techniques, the performance evaluation indexes in this paper adopt SNR and RMSE. SNR directly reflects the effect of the denoising method. The greater the SNR, the more effectively noise can be reduced and the better the denoising impact. The RMSE is used to compare the similarity of the denoised and original signals, and a lower error number implies a better denoising impact. The performance characteristics of each denoising approach are compared in (Table 1), and their SNR and RMSE expressions are as follows:

$$\mathrm{SNR} = 10\log_{10}\left\{\frac{\sum_{n=1}^{N} f^2(n)}{\sum_{n=1}^{N}\left(f(n) - \widetilde{f(n)}\right)^2}\right\} \tag{12}$$

$$\mathrm{RMSE} = \sqrt{\frac{1}{N}\sum_{n=1}^{N}\left[f(n) - \widetilde{f(n)}\right]^2} \tag{13}$$

where $f(n)$ is the signal before processing, $\widetilde{f(n)}$ is the signal after processing, and N is the length of the signal.

Table 1. Performance comparison of different denoising algorithms.

Denoising Method	Added Noise			
	10 dB		15 dB	
	SNR	RMSE	SNR	RMSE
Wavelet threshold denoising	20.1266	0.0986	22.3172	0.0766
CEEMDAN + Soft threshold denoising	19.9505	0.1005	21.7416	0.0818
CEEMDAN + Hard threshold denoising	21.4373	0.0947	23.8158	0.0644
CEEMDAN + Improved threshold denoising [39]	21.3067	0.0961	23.6247	0.0659
CEEMDAN + Improved threshold denoising [40]	20.8791	0.0973	23.2049	0.0691
Proposed Algorithm	21.8496	0.0908	25.5149	0.0531

From the data in (Table 1), it can be seen that when compared to single wavelet threshold denoising, CEEMDAN-wavelet soft threshold denoising, CEEMDAN-wavelet hard threshold denoising, literature 1 and literature 2, the CEEMDAN with improved wavelet threshold denoising algorithm proposed in this paper has the highest SNR, as well as the smallest RMSE, and has excellent denoising performance. With the addition of 15 dB of white noise, the denoising method proposed in this paper improves the SNR by 3.1977 dB and reduces the RMSE by 0.0235 over the conventional wavelet thresholding method.

The algorithm proposed in this paper is not only applicable to the electromyographic signals characterized by fish, but also has a better denoising effect on the electrical signals of other organisms. In order to verify the effectiveness and generalizability of the algorithm, the following supplementary simulation experiments were performed. A segment of human heart electrical signal [41] was selected from the public MIT-BIH database, where the sampling rate of the signal was 360 Hz. After adding 15 dB of noise to the original signal as a noise-containing signal (Figure 5A), it can be seen that the original signal is flooded with noise and loses its original signal characteristics. Noisy signals were processed using the denoising algorithms proposed in literature 1 [39], literature 2 [40] and in this study.

The original signal is uniformly represented by a specific color, as can be seen in (Figure 5B,C), after denoising reduction using the algorithms from literature 1 [39] and literature 2 [40], more details are lost and the denoised signal is too smooth and has a poor restoration. (Figure 5D) shows the denoising effect of the proposed algorithm in ECG signals, which can better restore the original signal from the noise-containing signals with noise interference, and the signal features can be better preserved.

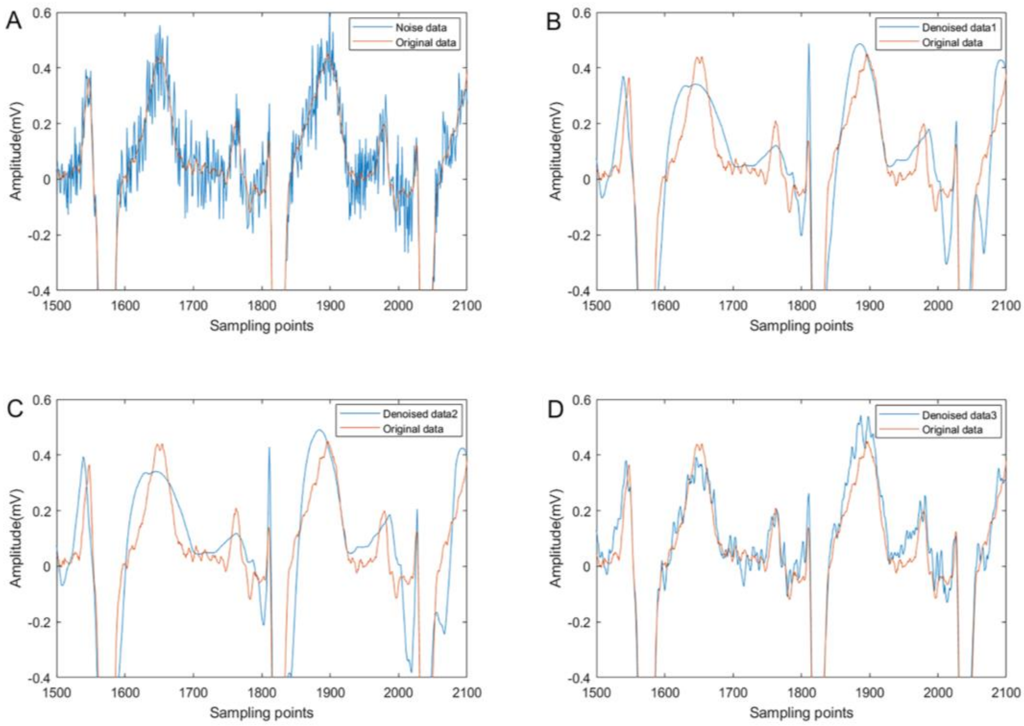

Figure 5. Comparison of the local noise reduction effects of processed human ECG signals under different denoising algorithms. Demonstration plot of the original signal with 15 dB of noise added (**A**), the original signal and the presentation graph after processing by the denoising algorithm in [39] (**B**), the original signal and the presentation graph after processing by the denoising algorithm in [40] (**C**), the original signal with the presentation plot after processing by the algorithm proposed in this paper (**D**).

As shown in (Table 2), the denoising quality is also visualized using SNR and RMSE. With 15 dB of noise added, literature 1 [39], literature 2 [40] have an SNR of 8.8071 and 7.5739 and an RMSE of 0.1661 and 0.1914. And the algorithm of this paper reaches an SNR of 12.8731 and an RMSE of 0.1121. Under the dual effect of signal decomposition selection and further improvement of the threshold function, the highest SNR and the lowest RMSE are obtained with the denoising algorithm of this paper, and the validity and universality of the algorithm are verified.

Table 2. Performance comparison of different denoising algorithms for processing human ECG.

Denoising Method	**Add Noise 15 dB**	
	SNR	**RMSE**
CEEMDAN + Improved threshold denoising [39]	8.8071	0.1661
CEEMDAN + Improved threshold denoising [40]	7.5739	0.1914
Proposed Algorithm	12.8731	0.1121

3.2. *Effect of Simulation Experiment*

The EMG of the tail of an adult crucian carp (452 g) during the tail-swinging behavior while gradually awakening form anesthesia with 80 μg/L eugenol solution was used. The recorded raw fish tail EMG signal is shown in (Figure 6). The unprocessed signal is prone to interference from trauma mucus and water flow fluctuations which adds a lot of noise. The fish physiological electrical signal itself is non-linear and non-smooth, which directly reduces the accuracy of the subsequent fish myoelectric signal analysis. This paper proposes that CEEMDAN with an improved wavelet thresholding method can be able to play a role in suppressing noise in subsequent signal processing.

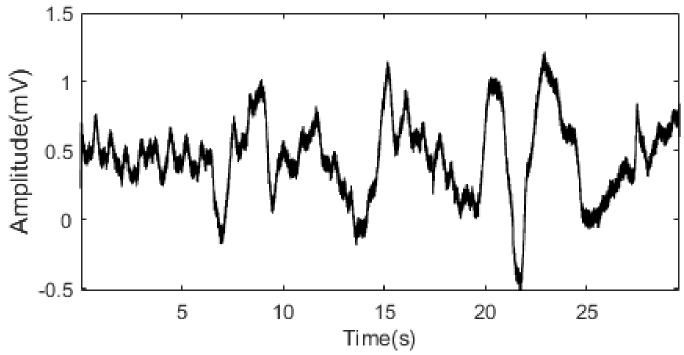

Figure 6. Time domain map of a raw unprocessed fish tail EMG signal.

3.2.1. CEEMDAN Decomposition

First, the fish EMG signal needs to be decomposed by CEEMDAN and it was concluded through several experiments that the result of adding the ratio of white noise standard deviation to the signal standard deviation being 0.2, the average signal number being 200, and the maximum number of iterations being 2000 works better. The 17 IMF and residual components were obtained from the original fish tail EMG signal by CEEMDAN decomposition, and the results are shown in (Figure 7).

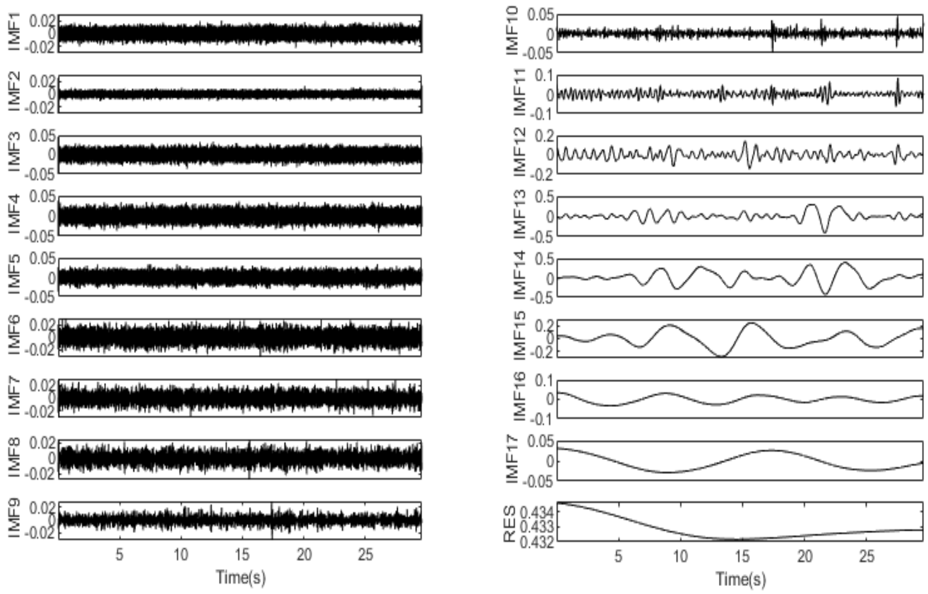

Figure 7. CEEMDAN decomposition of myoelectric signals in the tail of a fish.

3.2.2. Noise Treatment

Mutual correlation calculations were performed for each IMF with the original signal. The difference between the intercorrelation of each IMF and the number of intercorrelations of the previous IMF was calculated, and the difference curve was plotted as in (Figure 8). The second extreme point greater than zero, IMF1 and IMF2, was chosen as the critical point between the noise-dominated IMF component and the signal-dominated IMF component. The IMF14 with the largest number of interrelationships was selected in turn as the pure component, and the IMF9 with the smallest number of interrelationships is also used as the noise-dominated component, and all the noise-dominated IMFs were removed for the operation.

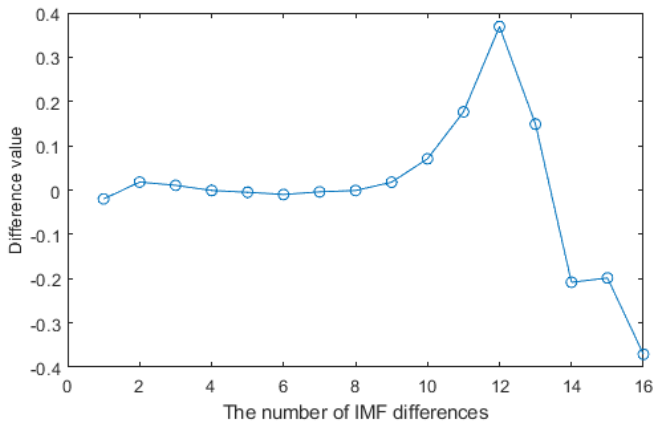

Figure 8. Difference curves derived from the number of correlations.

Improved wavelet threshold denoising was used for the remaining signal-dominated IMF. The wavelet basis function employed in this study, sym4, has a total of 5 decomposition layers, the preset parameters α and β were adjusted and superimposed on the IMF dominated by the signal after denoising using this method with the pure IMF. The denoised signal is shown in its final form in (Figure 9). The Sym4 wavelet has better symmetry and localization properties, which can better capture the local features of the signal. After experimental comparison with other wavelet bases, sym4 was found to be more suitable for fish EMG signal features. In the comparison between the denoised signal (Figure 9) and the original signal (Figure 6), we can see that the signal curve is smoother after the denoising process using CEEMDAN and the improved wavelet thresholding algorithm which suppresses the influence of strong noise on the signal and retains the real signal information.

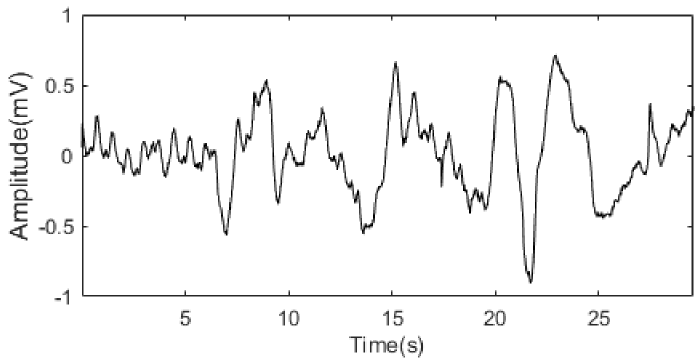

Figure 9. Signal-processed myoelectric signals from the tail of a fish.

4. Conclusions

This research proposes a signal processing method for denoising fish physiological electrical signals based on the combination of CEEMDAN and improved wavelet thresholding. Since there is no uniform standardization of the acquisition process for fish electrical signals, there are also large differences in the acquisition equipment, electrode implantation sites, and the acquisition environment. All of these factors can reduce the quality of the acquired fish electrical signals, and effective and generalizable signal preprocessing algorithms are necessary. The drawbacks of traditional thresholding functions, excessive smoothing, abrupt changes at the threshold and directly setting a small signal to zero, are all addressed by the improved wavelet thresholding function. The dual parameters that have been introduced can also be modified in accordance with the various waveform characteristics of the actual signal. The experimental results show that compared with the other denoising algorithms mentioned in this paper, the denoising algorithm proposed in this paper has a higher signal-to-noise ratio and lower root mean square error and can effectively suppress the noise in the signal. The method proposed in this paper focuses on fish physiological signal preprocessing which provides an effective signal denoising tool for in-depth analysis of fish behavior and physiological studies investigating the effects of certain states on fish behavior. Although this denoising algorithm can effectively improve the accuracy of the signal, there is still some room for optimization and improvement. In the future, on the one hand, it will be possible to continue to try to optimize and improve the signal quality in terms of pre-processing. On the other hand, we can try to establish a stronger link between the physiological electrical signals of fish and their own behaviors (e.g., opening and closing the mouth, wagging the tail, etc.) to differentiate specific fish behaviors from the perspective of electrophysiological signals.

Author Contributions: Conceptualization, J.M., W.C. and S.F.; methodology, J.M. and W.C.; validation, W.C., S.F. and B.Z.; formal analysis, J.M., S.O. and B.Z.; investigation, S.O., B.Z., W.C. and S.F.; resources, W.C., J.Z. and S.F.; writing—original draft preparation, J.M.; writing—review and editing, J.M., S.O. and W.C.; funding acquisition, W.C. All authors have read and agreed to the published version of the manuscript.

Funding: This research was funded by the National Natural Science Foundation of China [Grant 32073028], and Ningbo Youth Science and Technology Innovation Leading Talent Project [No. 2023QL004].

Data Availability Statement: Data available on request due to restrictions e.g., privacy or ethical. The data presented in this study are available on request from the corresponding author. The data are not publicly available due to their association with other research projects.

Conflicts of Interest: The authors declare no conflict of interest.

References

1. Wakeling, J.M. Biomechanics of fast-start swimming in fish. *Comp. Biochem. Physiol. A-Mol. Integr. Physiol.* **2001**, *131*, 31–40. [CrossRef]
2. Polnau, D.G.; Ma, P.A. Simultaneous video analysis of the kinematics of opercular movement and electromyographic activity during agonistic display in Siamese fighting fish. *Brain Res. Protoc.* **2001**, *8*, 228–235. [CrossRef] [PubMed]
3. Coughlin, D.J. Aerobic muscle function during steady swimming in fish. *Fish Fish.* **2002**, *3*, 63–78. [CrossRef]
4. Aydin, B.; Orhan, N. Effects of thymol and carvacrol anesthesia on the electrocardiographic and behavioral responses of the doctor fish Garra rufa. *Aquaculture* **2021**, *533*, 736134. [CrossRef]
5. Barbas, L.A.L.; Torres, M.F.; da Costa, B.M.P.; Feitosa, M.J.M.; Maltez, L.C.; Amado, L.L.; Toda, Y.P.S.; Batista, P.d.S.; Cabral, D.A.C.; Hamoy, M. Eugenol induces body immobilization yet evoking an increased neuronal excitability in fish during short-term baths. *Aquat. Toxicol.* **2021**, *231*, 105734. [CrossRef]
6. Lambooij, E.; Digre, H.; Reimert, H.G.M.; Aursand, I.G.; Grimsmo, L.; Van de Vis, J.W. Effects of on-board storage and electrical stunning of wild cod (*Gadus morhua*) and haddock (*Melanogrammus aeglefinus*) on brain and heart activity. *Fish. Res.* **2012**, *127*, 1–8. [CrossRef]
7. De Araújo, E.R.L.; da Silva e Silva, J.; Lopes, L.M.; Torres, M.F.; da Costa, B.M.P.A.; Amarante, C.B.D.; Hamoy, M.; Barbas, L.A.L.; Sampaio, L.A. Geraniol and citronellol as alternative and safe phytoconstituents to induce immobilization and facilitate handling of fish. *Aquaculture* **2021**, *537*, 736517. [CrossRef]
8. Barbas, L.A.L.; Hamoy, M.; de Mello, V.J.; Barbosa, R.P.M.; de Lima, H.S.T.; Torres, M.F.; Nascimento, L.A.S.D.; da Silva, J.K.D.R.; de Aguiar Andrade, E.H.; Gomes, M.R.F. Essential oil of citronella modulates electrophysiological responses in tambaqui *Colossoma macropomum*: A new anaesthetic for use in fish. *Aquaculture* **2017**, *479*, 60–68. [CrossRef]
9. Vilhena, C.S.; Nascimento, L.A.S.D.; Andrade, E.H.d.A.; da Silva, J.K.D.R.; Hamoy, M.; Torres, M.F.; Barbas, L.A.L. Essential oil of *Piper divaricatum* induces a general anaesthesia-like state and loss of skeletal muscle tonus in juvenile tambaqui, *Colossoma macropomum*. *Aquaculture* **2019**, *510*, 169–175. [CrossRef]
10. Da Costa, B.M.A.; Torres, M.F.; da Silva, R.A.; Aydın, B.; Amado, L.L.; Hamoy, M.; Barbas, L.A.L. Integrated behavioural, neurological, muscular and cardiorespiratory response in tambaqui, *Colossoma macropomum* anaesthetized with menthol. *Aquaculture* **2022**, *560*, 738553. [CrossRef]
11. Vieira, L.R.; Pereira, Y.L.G.; Diniz, L.A.; Nascimento, C.P.; Silva, A.L.M.; Azevedo, J.E.C.; de Mello, V.J.; Muto, N.A.; Barbas, L.A.L.; Hamoy, M. Graded concentrations of lidocaine hydrochloride in the modulation of behavioral, cardiac, and muscular responses of the Amazon freshwater fish tambaqui (*Colossoma macropomum*). *Aquaculture* **2023**, *563*, 738985. [CrossRef]
12. Ding, R.; Li, G.; Wang, Q. The method research on removing baseline wander of ECG. *J. Yunnan Univ. Nat. Sci.* **2014**, *36*, 655–660.

13. Echeverria, J.C.; Crowe, J.; Woolfson, M.S.; Hayes-Gill, B.R. Application of empirical mode decomposition to heart rate variability analysis. *Med. Biol. Eng. Comput.* **2001**, *39*, 471–479. [CrossRef]
14. Lu, L.; Niu, X.; Wang, J.; Li, C. ECG signal denoising based on EMD and statistical characteristics of IMF components. *Chin. J. Med. Phys.* **2021**, *38*, 1529–1534.
15. Huang, N.E.; Shen, Z.; Long, S.R.; Wu, M.C.; Shih, H.H.; Zheng, Q.; Yen, N.-C.; Tung, C.C.; Liu, H.H. The empirical mode decomposition and the Hilbert spectrum for nonlinear and non-stationary time series analysis. *Proc. R. Soc. A-Math. Phys. Eng. Sci.* **1998**, *454*, 903–995. [CrossRef]
16. Kopsinis, Y.; McLaughlin, S. Development of EMD-Based Denoising Methods Inspired by Wavelet Thresholding. *IEEE Trans. Signal Process.* **2009**, *57*, 1351–1362. [CrossRef]
17. Andrade, A.O.; Nasuto, S.; Kyberd, P.; Sweeney-Reed, C.M.; Van Kanijn, F. EMG signal filtering based on Empirical Mode Decomposition. *Biomed. Signal Process. Control* **2006**, *1*, 44–55. [CrossRef]
18. Han, G.; Lin, B.; Xu, Z. Electrocardiogram signal denoising based on empirical mode decomposition technique: An overview. *J. Instrum.* **2017**, *12*, P03010. [CrossRef]
19. Kabir, M.A.; Shahnaz, C. Denoising of ECG signals based on noise reduction algorithms in EMD and wavelet domains. *Biomed. Signal Process. Control* **2012**, *7*, 481–489. [CrossRef]
20. Tang, B.; Dong, S.; Song, T. Method for eliminating mode mixing of empirical mode decomposition based on the revised blind source separation. *Signal Process.* **2012**, *92*, 248–258. [CrossRef]
21. Wu, Z.; Huang, N. Ensemble empirical mode decomposition: A noise-assisted data analysis method. *Adv. Adapt. Data Anal.* **2009**, *1*, 1–41. [CrossRef]
22. Torres, M.E.; Colominas, M.A.; Schlotthauer, G.; Flandrin, P. A complete ensemble empirical mode decomposition with adaptive noise. In Proceedings of the IEEE International Conference on Acoustics, Speech, and Signal Processing (ICASSP), Prague, Czech Republic, 22–27 May 2011.
23. Hu, Y.; Ouyang, Y.; Wang, Z.; Yu, H.; Liu, L. Vibration signal denoising method based on CEEMDAN and its application in brake disc unbalance detection. *Mech. Syst. Signal Process.* **2023**, *187*, 109972. [CrossRef]
24. Zhou, H.; Yan, P.; Yuan, Y.; Wu, D.; Huang, Q. Denoising the hob vibration signal using improved complete ensemble empirical mode decomposition with adaptive noise and noise quantization strategies. *Isa Trans.* **2022**, *131*, 715–735. [CrossRef]
25. Yang, Y.; Li, S.; Li, C.; He, H.; Zhang, Q. Research on ultrasonic signal processing algorithm based on CEEMDAN joint wavelet packet thresholding. *Measurement* **2022**, *201*, 111751. [CrossRef]
26. Yao, L.; Pan, Z. A new method based CEEMDAN for removal of baseline wander and powerline interference in ECG signals. *Optik* **2020**, *223*, 165566. [CrossRef]
27. Lou, H.S.; Hang, H.; Li, J.; Shi, C. Research on denoising algorithm of rain signal based on improved CEEMDAN and wavelet threshold. *Electron. Meas. Technol.* **2023**, *46*, 103–109.
28. Beni, N.H.; Jiang, N. Heartbeat detection from single-lead ECG contaminated with simulated EMG at different intensity levels: A comparative study. *Biomed. Signal Process. Control* **2023**, *83*, 104612. [CrossRef]
29. Zhang, N. The Application of an Improved Wavelet Threshold Function in De-noising of Heart Sound Signal. In Proceedings of the 32nd Chinese Control and Decision Conference (CCDC), Hefei, China, 22–24 August 2020.
30. Fei, H.; Shan, J. Application of CEEMDAN-Wavelet Threshold Method in Blasting Vibration Signal Processing. *Blasting* **2022**, *39*, 41–47.
31. Gao, L.; Gan, Y.; Shi, J. A novel intelligent denoising method of ecg signals based on wavelet adaptive threshold and mathematical morphology. *Appl. Intell.* **2022**, *52*, 10270–10284. [CrossRef]
32. Cui, G.; Zhang, Z.; Yang, L. An improved wavelet threshold denoising algorithm. *Mod. Electron. Tech.* **2019**, *42*, 50–53+58.
33. Duan, Q.; Li, F.; Tian, Z. An Improved Method for Wavelet Thresholding Signal Denoising. *Comput. Simul.* **2009**, *26*, 348–351.
34. Liu, W.D.; Liu, S.H.; Hu, X.F.; Wang, L. Analysis of Modified Methods of Wavelet Threshold De-noising Functions. *High Volt. Eng.* **2007**, *33*, 59–63.
35. Sun, D.; Ou, T. Research on Denoising Method of Groundwater Temperature Observation Data Using the Improved Wavelet Threshold Denoising Combined with CEEMDAN. *J. Geod. Geodyn.* **2023**, *43*, 435–440.
36. Qin, A.; Dai, L. A Speech Enhancement Algorithm Based on Improved Wavelet Threshold Function. *J. Hunan Univ. Nat. Sci.* **2015**, *42*, 136–140.
37. Ma, H.; Lu, W.; Geng, S. Research on wavelet denoising method based on improved threshold function. *Laser J.* **2023**, *44*, 19–24.
38. Luo, H.; Liu, Y.; Gan, Y.; Li, N.; Jiang, H.; Zhu, Z.; Xie, K. An OTDR signal denoising algorithm based on CEEMDAN improved wavelet threshold. *J. Optoelectron. Laser* **2022**, *33*, 241–247.
39. Sun, W.; Wang, C. Power signal denoising based on improved soft threshold wavelet packet network. *J. Nav. Univ. Eng.* **2019**, *31*, 79–82.
40. Zhang, P.; Li, X.; Cui, S. An improved wavelet threshold-CEEMDAN algorithm for ECG signal denoising. *Comput. Eng. Sci.* **2020**, *42*, 2067–2072.
41. Moody, G.B.; Mark, R.G. The impact of the MIT-BIH Arrhythmia Database. *IEEE Eng. Med. Biol.* **2001**, *20*, 45–50. [CrossRef]